KANAZAWA-13-02

A two-loop Radiative Seesaw with multi-component Dark Matter explaining the possible γ Excess in the Higgs decay and at the Fermi LAT

Mayumi Aoki,[1,2,*] Jisuke Kubo,[1,†] and Hiroshi Takano[1,‡]

[1] *Institute for Theoretical Physics, Kanazawa University, Kanazawa 920-1192, Japan*

[2] *Max–Planck–Institut für Kernphysik, Saupfercheckweg 1, 69117 Heidelberg, Germany*

Abstract

A non-supersymmetric model of two-loop radiative seesaw is proposed. The model contains, in addition to the standard model (SM) Higgs boson, an inert $SU(2)_L$ doublet scalar η and two inert singlet scalars ϕ and χ. The lepton number is softly broken by a dimension two operator, and the tree-level Dirac mass is forbidden by $Z_2 \times Z_2'$ (or D_{2N}) , which predicts the existence of two or three dark matter particles. The scalar sector is minimal; none of the scalar fields can be suppressed for the radiative seesaw mechanism to work. There are by-products: The SM Higgs boson decay into two γ's is slightly enhanced by η^+ (the charged component of η) circulating in one-loop diagrams for $h \to \gamma\gamma$. The 135 GeV γ-ray line observed at the Fermi LAT can be also explained by the annihilation of χ dark matter. We employ a mechanism of temperature-dependent annihilation cross section to suppress the continuum γ-rays and the production of anti-protons. The explanation can survive even down to the XENON1T sensitivity limit.

PACS numbers: 95.35.+d, 95.85.Pw, 11.30.Er

*Electronic address: mayumi@hep.s.kanazawa-u.ac.jp

†Electronic address: jik@hep.s.kanazawa-u.ac.jp

‡Electronic address: takano@hep.s.kanazawa-u.ac.jp

I. INTRODUCTION

Why the neutrino masses are small is a long-standing mystery. The seesaw mechanism [1–3] is an approach to provide an answer to it. The traditional seesaw mechanism indicates the existence of a superhigh scale physics beyond the standard model (SM). Another way to confront this problem is to generate the neutrino masses radiatively [4–6]. Many models have been proposed on the basis of the radiative generation of the neutrino masses, and the idea of the radiative seesaw mechanism [7, 8] is along the line of this idea: Right-handed neutrinos are introduced, but the Dirac masses are forbidden by a discrete symmetry. This discrete symmetry can be an origin of stable dark matter (DM) particles [7–11] in the universe.

To produce the neutrino masses, the lepton number L has to be violated. In most of the models the lepton number L is violated softly by dimension three operators, Majorana masses or scalar tri-linear couplings, and the number of the loops is ranging from one to three (see [12] for different models). For the radiative seesaw mechanism, the number of loops ℓ means a scaling down of $(1+3\ell)$ orders of magnitude for the right-handed neutrino mass (see also the discussions of [13]); $(\kappa/16\pi^2)^\ell \simeq (\kappa/0.1)\times 6.3\times 10^{-4}$, $(\kappa/0.1)^2\times 4.0\times 10^{-7}$, $(\kappa/0.1)^3\times 2.5\times 10^{-10}$ for $\ell = 1$, 2 and 3, respectively, where κ is a generic coupling. Since the Majorana mass of the right-handed neutrino for the tree-level seesaw is $O(10^{10})$ GeV, we may obtain a Majorana mass of $O(1)$ TeV naturally in two-loop radiative seesaw models [14, 15].

In this paper we propose a radiative seesaw model, in which the lepton number is softly broken by a dimension two operator, and the neutrino masses are generated at the two-loop level. The discrete symmetry is $Z_2\times Z_2'$ (or D_{2N} with $N = 2, 3, \ldots$ [1]). Therefore, two or three DM particles can exist in this model [2]. Obviously, radiative generation of the neutrino masses means an extension of the SM Higgs sector, which may have impacts on the existing experiments. In our model, we have a set of an inert doublet scalar η, and two singlet scalars. This set is minimal in the sense that the radiative neutrino mass generation does not work if one of them is suppressed. So, none of the extra scalar fields is ad hoc introduced. The existence of additional scalar doublets can change the decay rates of the SM Higgs boson h. The results of LHC indicate a slight excess of $h\to\gamma\gamma$ [20–22] which in fact could be explained by an additional inert doublet circulating in one-loop [23–26].

There is yet another excess of γ at the Fermi Large Area Telescope (LAT) [27–30]. There are analyses [31–36] that indicate a monochromatic γ-ray line of 135 GeV in the Fermi data. It has been reported [37] that a two-component DM system consisting of an inert doublet scalar and a scalar can explain the monochromatic γ-ray line at Fermi LAT. Different models with a two-component DM have been also considered in [38, 39] to explain

[1] D_{2N} (the dihedral group of order $2N$) is larger than $Z_2\times Z_2'$. However, we use only the one-dimensional representations of D_{2N} so that D_{2N} acts as $Z_2\times Z_2'$.

[2] Multicomponent DM system has been considered recently in [16–19], and see the references therein.

TABLE I: The matter content of the model and the corresponding quantum numbers. $Z_2 \times Z_2'$ is the unbroken discrete symmetry, while the lepton number L is softly broken by the ϕ mass. D_{2N} $(N = 2, 3, \ldots)$ is the dihedral group of order $2N$.

field	statistics	$SU(2)_L$	$U(1)_Y$	L	Z_2	Z_2'	D_{2N}
$L = (\nu_L, l_L)$	F	2	$-1/2$	1	+	+	$\mathbf{1}$
l_R^c	F	1	1	1	+	+	$\mathbf{1}$
N_R^c	F	1	1	0	−	+	$\mathbf{1''}$
$H = (H^+, H^0)$	B	2	1/2	0	+	+	$\mathbf{1}$
$\eta = (\eta^+, \eta^0)$	B	2	1/2	-1	−	+	$\mathbf{1''}$
χ	B	1	0	0	+	−	$\mathbf{1'}$
ϕ	B	1	0	1	−	−	$\mathbf{1'''}$

the monochromatic Fermi LAT γ-ray line. Therefore it is natural to wonder whether our two-loop radiative seesaw model can explain the γ excess in the Higgs boson decay as well as at the Fermi LAT [3]. We find that this is in fact possible if we accept that certain scalar couplings are large at the border of perturbation theory, where to suppress sufficiently the continuum γ's and the production of anti-protons, we employ a mechanism of temperature-dependent annihilation cross section [44].

II. THE MODEL

The matter content of the model is shown in Table I. The new fields are (in addition to the right-handed neutrino N_R^c): $SU(2)_L$ doublet scalar η (L$= -1$), and singlet scalars χ (L$= 0$) and ϕ (L$= 1$), where L is the lepton number. Note that L of N_R^c is zero and that four different representations of $Z_2 \times Z_2'$ are exactly the singlets of the dihedral group of order $2N$, D_{2N} $(N = 2, 3, \ldots)$. The $Z_2 \times Z_2' \times$ L -invariant (or $D_{2N} \times$ L -invariant) Yukawa couplings of the lepton sector can be described by

$$\mathcal{L}_Y = Y_{ij}^e H^\dagger L_i l_{Rj}^c + Y_{ik}^\nu L_i \epsilon \eta N_{Rk}^c + h.c. \tag{1}$$

with the Majorana mass term of the right-handed neutrinos N_{Rk}^c $(k = 1, 2, 3)$

$$\mathcal{L}_{\rm Maj} = -\frac{1}{2}[\, M_k N_{Rk}^c N_{Rk}^c + h.c.\,]\ . \tag{2}$$

The most general form of the $Z_2 \times Z_2' \times$ L-invariant scalar potential is given by

$$V_\lambda \ = \ \lambda_1 (H^\dagger H)^2 + \lambda_2 (\eta^\dagger \eta)^2 + \lambda_3 (H^\dagger H)(\eta^\dagger \eta) + \lambda_4 (H^\dagger \eta)(\eta^\dagger H)$$

[3] Recently, it has been argued that the monochromatic γ-ray line can be explained basically by the same one-loop contribution as for $h \to \gamma\gamma$ [37, 40–43].

$$+\gamma_1\chi^4+\gamma_2(H^\dagger H)\chi^2+\gamma_3(\eta^\dagger\eta)\chi^2+\gamma_4|\phi|^4+\gamma_5(H^\dagger H)|\phi|^2$$
$$+\gamma_6(\eta^\dagger\eta)|\phi|^2+\gamma_7\chi^2|\phi|^2+\frac{\kappa}{2}[\,(H^\dagger\eta)\chi\phi+h.c.\,]\ . \tag{3}$$

Note that the "λ_5 term", $(1/2)\lambda_5(H^\dagger\eta)^2$, is forbidden by L. The $Z_2\times Z_2'$- invariant mass term is

$$V_m\ =\ m_1^2H^\dagger H+m_2^2\eta^\dagger\eta+\frac{1}{2}m_3^2\chi^2+m_4^2|\phi|^2+\frac{1}{2}m_5^2[\,\phi^2+(\phi^*)^2\,]\ , \tag{4}$$

where the last term in (4) breaks L softly. This is the only $Z_2\times Z_2'$ -invariant mass term which can break L softly. In the absence of this term, there will be no neutrino mass. The charged, CP even and odd scalars are defined as

$$H\ =\ \begin{pmatrix} H^+ \\ (v_h+h+iG)/\sqrt{2}\end{pmatrix}\ ,\ \eta=\begin{pmatrix}\eta^+\\(\eta_R^0+i\eta_I^0)/\sqrt{2}\end{pmatrix}\ ,\ \phi=(\phi_R+i\phi_I)/\sqrt{2}\ . \tag{5}$$

The tree-level masses of the scalars are given by

$$\begin{aligned} m_h^2\ &=\ 2\lambda_1v_h^2\ ,\ m_{\eta^\pm}^2=m_2^2+\frac{1}{2}\lambda_3v_h^2\ ,\ m_{\eta_R^0}^2=m_{\eta_I^0}^2=m_2^2+\frac{1}{2}(\lambda_3+\lambda_4)v_h^2\ , \\ m_{\phi_R}^2\ &=\ m_4^2+m_5^2+\gamma_5v_h^2\ ,\ m_{\phi_I}^2=m_4^2-m_5^2+\gamma_5v_h^2\ ,\ m_\chi^2=m_3^2+\gamma_2v_h^2\ . \end{aligned} \tag{6}$$

A. Stability of the vacuum

The potential V_λ is unbounded below if

$$\lambda_1\ ,\ \lambda_2\ ,\ \gamma_1\ ,\ \gamma_4>0\ , \tag{7}$$
$$\lambda_3>-\frac{2}{3}\sqrt{\lambda_1\lambda_2}\ ,\lambda_3+\lambda_4>-\frac{2}{3}\sqrt{\lambda_1\lambda_2}\ , \tag{8}$$
$$\gamma_2>-\frac{2}{3}\sqrt{\lambda_1\gamma_1}\ ,\ \ \gamma_5>-\frac{2}{3}\sqrt{\lambda_1\gamma_4}\ ,\ \ \gamma_3>-\frac{2}{3}\sqrt{\lambda_2\gamma_1}\ , \tag{9}$$
$$\gamma_6>-\frac{2}{3}\sqrt{\lambda_2\gamma_4}\ ,\ \gamma_7>-\frac{2}{3}\sqrt{\gamma_1\gamma_4}\ , \tag{10}$$
$$\lambda_1+\lambda_2+\gamma_1+\gamma_4-\frac{2}{3}\left(\sqrt{\lambda_1\lambda_2}+\sqrt{\lambda_1\gamma_1}+\sqrt{\lambda_1\gamma_4}\right.$$
$$\left.+\sqrt{\lambda_2\gamma_1}+\sqrt{\lambda_2\gamma_4}+\sqrt{\gamma_1\gamma_4}\right)>|\kappa| \tag{11}$$

are satisfied. The minimum of V_λ is zero if the inequalities above are satisfied. The discrete symmetry $Z_2\times Z_2'$ (or D_{2N}) is unbroken if, in addition to (7)-(11), the inequalities $m_2^2\ ,\ m_3^2\ ,\ m_4^2$ and $m_4^2-|m_5|^2>0$ are satisfied.

The inequalities (7)-(11) are sufficient conditions, but not necessary ones. If we assume that (7) and $\gamma_2,\gamma_3,\gamma_5,\gamma_6,\gamma_7>0$ are satisfied, for instance, the inequalities (8) are relaxed to

$$\lambda_3\ ,\ \lambda_3+\lambda_4>-2\sqrt{\lambda_1\lambda_2}\ , \tag{12}$$

and (11) is relaxed to

$$\lambda_1 + \lambda_2 + \gamma_1 + \sum_{i=2}^{7} \gamma_i - 2\sqrt{\lambda_1 \lambda_2} > |\kappa| \ . \tag{13}$$

Since $m_h = 125$ GeV and $v_h = 246$ GeV, the Higgs coupling λ_1 is fixed at 0.129. Then (12) implies that

$$\lambda_3 \ , \ \lambda_3 + \lambda_4 \ > \ -2.5\sqrt{\lambda_2/4\pi}. \tag{14}$$

B. Neutrino mass

The neutrino masses can be generated at the two-loop level as shown in Fig. 1. The mechanism of the radiative generation is the following. Because of the soft breaking of the dimension two operator ϕ^2, the propagator between ϕ and ϕ can exist. This can generate a $\eta^0\eta^0$ mass term. In the one-loop radiative seesaw model of [8] this mass is generated at the tree-level through the "λ_5" coupling. So the effective $\lambda_5^{\rm eff}$ is

$$\lambda_5^{\rm eff} \ = \ -\frac{\kappa^2}{64\pi^2}\left[\frac{m_{\phi_I}^2}{m_{\phi_I}^2 - m_\chi^2}\ln\frac{m_{\phi_I}^2}{m_\chi^2} - \frac{m_{\phi_R}^2}{m_{\phi_R}^2 - m_\chi^2}\ln\frac{m_{\phi_R}^2}{m_\chi^2}\right] \ . \tag{15}$$

Therefore, $\lambda_5^{\rm eff}$ can not be large within the framework of perturbation theory ($\lambda_5^{\rm eff} \lesssim O(10^{-3})$). The two-loop neutrino mass matrix is calculated to be

$$\begin{aligned}(\mathcal{M}_\nu)_{ij} \ &= \ \left(\frac{1}{16\pi^2}\right)^2 \frac{\kappa^2 v_h^2}{8}\sum_k Y_{ik}^\nu Y_{jk}^\nu M_k \ \int_0^\infty dx\{ \ B_0(-x, m_\chi, m_{\phi_R}) - B_0(-x, m_\chi, m_{\phi_I}) \ \} \\ &\quad \times \frac{x}{(x+m_\eta^2)^2(x+M_k^2)} \ \ \text{for } m_\eta = m_{\eta_R^0} \simeq m_{\eta_I^0} \qquad (16) \\ &\sim \ -\lambda_5^{\rm eff} v_h^2 \sum_k \frac{Y_{ik}^\nu Y_{jk}^\nu}{16\pi^2 M_k}\left(\ln\left(\frac{m_{\eta_R^0}}{M_k}\right)^2 + 1\right) \text{for } m_\eta \ll M_k \ , \qquad (17)\end{aligned}$$

where the function B_0 is the Passarino-Veltman function [45]

$$\frac{i}{16\pi^2}B_0(p^2, m_1, m_2) = \int \frac{d^D k}{(2\pi)^D}\frac{1}{(k^2 - m_1^2 + i\epsilon)((k+p)^2 - m_2^2 + i\epsilon)} \ , \tag{18}$$

and to obtain (17) we have used the one-loop mass formula with the effective coupling (15) [4]. Therefore, the scale of the light neutrino mass will be

$$\frac{\kappa^2}{64\pi^2}\frac{1}{16\pi^2}\frac{m_D^2}{M} \sim \left(\frac{\kappa}{0.1}\right)^2 10^{-7} \times \frac{m_D^2}{M} \ , \tag{19}$$

where m_D^2/M is the scale in the case of the tree-level Type-I seesaw. This means that we can scale down the mass of the right-handed neutrino by seven orders of magnitude. So, the right-handed neutrino masses of TeV or less are naturally expected in this model.

[4] There is $O(1)$ correction to the approximate formula (17) which we have checked numerically.

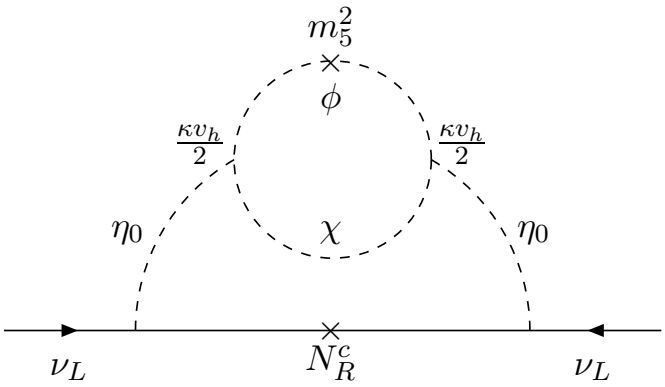

FIG. 1: Two-loop radiative neutrino mass.

C. Constraints

1: $\underline{\mu \to e\,\gamma}$
The constraint coming from $\mu \to e\gamma$ is given by [46]

$$B(\mu \to e\gamma) = \frac{3\alpha}{64\pi (G_F m_{\eta^\pm}^2)^2} \left| \sum_k Y_{\mu k}^\nu Y_{ek}^\nu F_2\left(\frac{M_k^2}{m_{\eta^\pm}^2}\right)\right|^2 \lesssim 2.4\times 10^{-12}\ , \tag{20}$$
$$F_2(x) = \frac{1}{6(1-x)^4}(1-6x+3x^2+2x^3-6x^2\ln x)\ ,$$

where the upper bound is taken from [47]. A similar, but slightly weaker bound for $\tau \to \mu(e)\gamma$ given in [47] has to be satisfied, too. Since $F_2(x) \sim 1/3x$ for $x \gg 1$, while $1/12 < F_2(x) < 1/6$ for $0 < x < 1$, the constraint can be readily satisfied if $M_k \ll m_{\eta^\pm}$ or $M_k \gg m_{\eta^\pm}$. If we assume that $M_1 = M_2 = M_3 = 1$ TeV $\gg m_{\eta^\pm}$ in (20), the constraint (20) becomes $B(\mu \to e\gamma) \simeq 10^{-7} \times \sum_k Y_{\mu k}^\nu Y_{ek}^\nu \lesssim 2.4\times 10^{-12}$. Therefore, $Y_{ek}^\nu Y_{\mu k}^\nu \lesssim O(10^{-5})$ can satisfy the constraint. This size is also the right size to obtain light neutrino masses of a correct order.

2: $\underline{g_\mu - 2}$
The extra contribution to the anomalous magnetic moment of the muon, $a_\mu = (g_\mu - 2)/2$, is given by [46]

$$\delta a_\mu \ = \ \frac{m_\mu^2}{16\pi^2 m_{\eta^\pm}^2} \sum_k Y_{\mu k}^\nu Y_{\mu k}^\nu F_2\left(\frac{M_k^2}{m_{\eta^\pm}^2}\right)\ . \tag{21}$$

If we assume that $|\sum_k Y_{\mu k}^\nu Y_{\mu k}^\nu F_2\left(\frac{M_k^2}{m_{\eta^\pm}^2}\right)| \simeq |\sum_k Y_{\mu k}^\nu Y_{ek}^\nu F_2\left(\frac{M_k^2}{m_{\eta^\pm}^2}\right)|$, then we obtain

$$|\delta a_\mu| \ \simeq \ 2.2\times 10^{-5} B(\mu \to e\gamma) \lesssim 3.4\times 10^{-11} \tag{22}$$

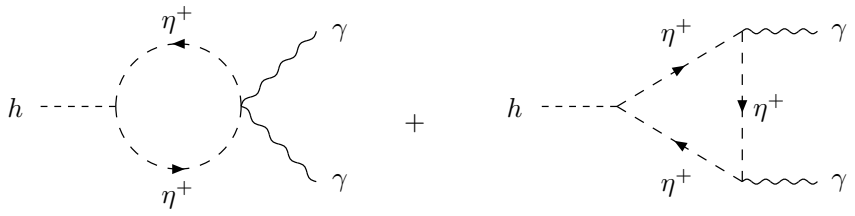

FIG. 2: One-loop diagrams for $h \to \gamma\gamma$.

if (20) is satisfied, where the upper bound is taken from [48]. So, the constraint from a_μ has no significant influence.

3: Electroweak precision
The electroweak precision measurement requires [48, 49]

$$\Delta T \simeq 0.54 \left(\frac{m_{\eta^\pm} - m_{\eta_R^0}}{v}\right)\left(\frac{m_{\eta^\pm} - m_{\eta_I^0}}{v}\right) = 0.02^{+0.11}_{-0.12} \tag{23}$$

for $m_h = 115$ – 127 GeV. Therefore, $|m_{\eta^\pm} - m_{\eta_R^0}|$, $|m_{\eta^\pm} - m_{\eta_I^0}| \lesssim 100$ GeV is sufficient to meet the requirement.

III. DM AND RESTRICTING THE PARAMETER SPACE

A. $h \to \gamma\gamma$

Because of the coupling $\mathcal{L}_{H^\dagger H \eta^\dagger \eta} = -\lambda_3 (H^\dagger H)(\eta^\dagger \eta) = -\lambda_3 v_h h \eta^+ \eta^- + \cdots$, there are additional diagrams that contribute to the one-loop decay $h \to \gamma\gamma$, which are shown in Fig. 2. Therefore, the decay width for two γ's can be increased [23–26]:

$$\begin{aligned}
\frac{\Gamma(\gamma\gamma)}{\Gamma^{\rm SM}(\gamma\gamma)} &= \left[\frac{3(3/2)^2 F_{1/2}(\tau_t) + F_1(\tau_W) + 2\lambda_3 (m_W^2/g^2 m_{\eta^\pm}^2) F_0(\tau_{\eta^\pm})}{3(3/2)^2 F_{1/2}(\tau_t) + F_1(\tau_W)}\right]^2 , \\
\tau_t &= 4m_t^2/m_h^2,\ \tau_W = 4m_W^2/m_h^2 ,\ \tau_{\eta^\pm} = 4m_{\eta^\pm}^2/m_h^2 , \\
F_{1/2}(\tau) &= 2 + 3\tau + 3\tau(2-\tau)\arcsin^2(1/\sqrt{\tau}) , \\
F_1(\tau) &= -2\tau[1 + (1-\tau)\arcsin^2(1/\sqrt{\tau})] , \\
F_0(\tau) &= \tau[1 - \tau \arcsin^2(1/\sqrt{\tau})] ,
\end{aligned} \tag{24}$$

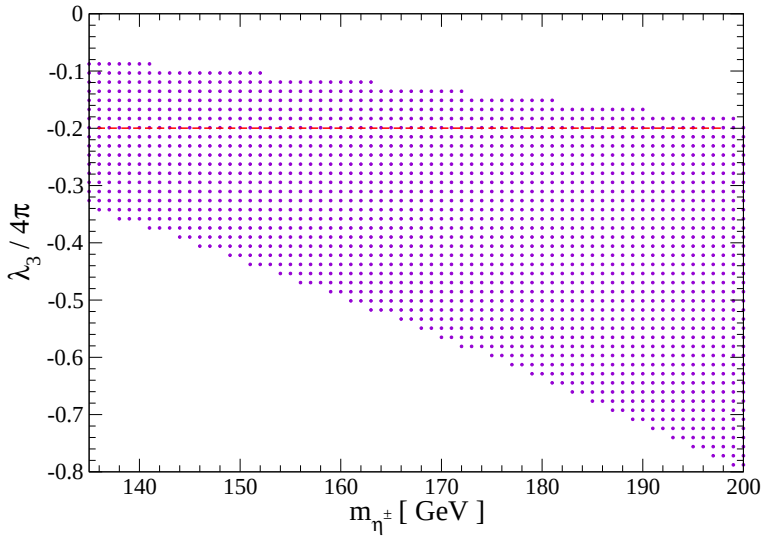

FIG. 3: The area with $\Gamma/\Gamma^{\rm SM} = 1.6 \pm 0.4$ in the $m_{\eta^\pm}$–λ_3 plane. The horizontal red line is the stability bound in given in (14).

where $\arcsin^2(1/\sqrt{\tau})$ should be replaced by $(-1/4)[\ln \frac{1+\sqrt{1+\tau}}{1-\sqrt{1-\tau}} - i\pi]^2$ for $\tau < 1$. We obtain

$$\frac{\Gamma(\gamma\gamma)}{\Gamma^{\rm SM}(\gamma\gamma)} \simeq \begin{cases} 1.20 & 1.31 & 1.54 \\ 1.17 & 1.26 & 1.45 \\ 1.16 & 1.24 & 1.42 \\ 1.05 & 1.12 & 1.22 \end{cases} \text{ for } \lambda_3 = -\{\ 1\ \ 1.5\ \ 2.5 \text{ and } m_{\eta\pm} = \begin{cases} 135 \\ 145 \\ 150 \\ 200 \end{cases} \text{ GeV .} \quad (25)$$

So, if the charged inert scalar η^+ is relatively light and λ_3 is negative and large, the observed excess 1.6 ± 0.4 in the CMS experiment [21] can be explained. (The best fit signal strength for this mode in the ATLAS experiment [20, 22] is $\hat{\mu} = 1.9 \pm 0.5$.) In Fig. 3 we show the area in the $m_{\eta^\pm}$–λ_3 plane in which $\Gamma(\gamma\gamma)/\Gamma^{\rm SM}(\gamma\gamma) = 1.6 \pm 0.4$ can be obtained [5] As we can see from (8), a large negative λ_3 may endanger the vacuum stability, because λ_1 is fixed at 0.129. Therefore, we assume that all the quartic scalar couplings except λ_3 and λ_4 are positive and use the second set of the inequality conditions (12) and (13). (14) means that $\lambda_3 \gtrsim -2.5$ if λ_2 is at the border of perturbation theory. Thus, the Higgs boson decay mode $h \to \gamma\gamma$ prefers the parameter space:

1. All the quartic scalar couplings except λ_3 and λ_4 are positive and λ_2 is large, and

2. the constraints

$$-0.2 \lesssim \lambda_3/4\pi \lesssim -0.08 \text{ and } m_{\eta^\pm} \lesssim 200 \text{ GeV .} \quad (26)$$

[5] The upper bound $m_{\eta^\pm} < 135$ GeV given in [26] is obtained from $\Gamma(\gamma\gamma)/\Gamma^{\rm SM}(\gamma\gamma) > 1.3$ and $\lambda_3/4\pi > -1.46/4\pi \simeq -0.116$, which is consistent with (25). Note that we use $2.0 \geq \Gamma(\gamma\gamma)/\Gamma^{\rm SM}(\gamma\gamma) \geq 1.2$ for Fig. 3 along with the stability constraint (14).

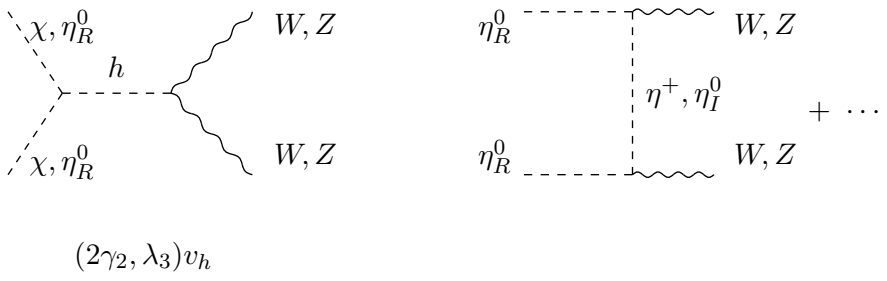

FIG. 4: Tree-level DM annihilations into W^+W^- and ZZ.

have to be satisfied.

B. Direct Detection of DM

As we can see from Table I, either N_R^c or η can be a DM candidate. Here we assume that η_R^0, the CP even component of η, is a DM particle and assume that $M_k \gg m_{\eta_R^0}$, $m_{\eta_I^0}$, $m_{\eta^\pm}$ to satisfy the $\mu \to e\gamma$ constraint (20). The model can have three stable DM particles in principle, but to simplify the situation we assume a two-component DM system. Another one is either χ or ϕ. As we see from the potential (3), there is no significant difference between χ and ϕ as DM. So we assume here that χ is the second DM particle.

The spin-independent elastic cross section off the nucleon $\sigma(\chi(\eta_R^0))$ is given by [49]

$$\sigma(\chi(\eta_R^0)) \;=\; \frac{1}{\pi}\left(\frac{\gamma_2(\lambda_L/2)\hat{f}m_N}{m_{\chi(\eta_R^0)}m_h^2}\right)^2\left(\frac{m_N m_{\chi(\eta_R^0)}}{m_N + m_{\chi(\eta_R^0)}}\right)^2 , \tag{27}$$

where $\lambda_L = \lambda_3 + \lambda_4$, m_N is the nucleon mass, and $\hat{f} \sim 0.3$ stems from the nucleonic matrix element [50]. The cross sections have to satisfy

$$\left(\frac{\sigma(\chi)}{\sigma_{\rm UB}(m_\chi)}\right)\left(\frac{\Omega_\chi h^2}{\Omega_T h^2}\right) + \left(\frac{\sigma(\eta_R^0)}{\sigma_{\rm UB}(m_{\eta_R^0})}\right)\left(\frac{\Omega_\eta h^2}{\Omega_T h^2}\right) \lesssim 1 , \tag{28}$$

where $\Omega_T h^2 = 0.116$ [51] and $\sigma_{\rm UB}(m) \simeq 3 \times 10^{-45}$ cm^2 [52] is the XENON100 limit for the DM mass of 135 GeV. So, we find

$$|\gamma_2| \;\lesssim\; 0.035\ (0.003) \text{ if } \Omega_\chi h^2 \simeq \Omega_T h^2 = 0.116 \text{ and } m_\chi = 135 \text{ GeV} , \tag{29}$$

$$|\lambda_3 + \lambda_4| \;\lesssim\; 0.069\ (0.006) \text{ if } \Omega_\eta h^2 \simeq \Omega_T h^2 = 0.116 \text{ and } m_{\eta_R^0} = 135 \text{ GeV} , \tag{30}$$

where we would obtain the numbers in the parentheses when the XENON1T sensitivity $\sigma \sim 2 \times 10^{-47}$ cm^2 [53] would has been reached. Because of (26) we have to assume a large negative λ_3, and, because of $m_{\eta^\pm}^2 - m_{\eta_R^0}^2 = -\lambda_4 v_h^2/2$, λ_4 has to be negative, too, to

ensure $m_{\eta^\pm} > m_{\eta_R^0}$. If λ_4 is negative and in addition λ_3 is large and negative, the inequality (12) may be violated, unless λ_4 is small and negative. This means $\lambda_L \simeq \lambda_3$, implying that (30) can not be satisfied. Therefore, the relic density of η_R^0 has to be small to satisfy the constraint (28). This is welcome, because the annihilation cross section of η_R^0 is large in general due to the gauge interactions shown in Fig. 4 [54–56]. Thus, the parameter space is further constrained to:

1. λ_4 has to be negative and small to ensure $m_{\eta^\pm} > m_{\eta_R^0}$ and to satisfy the constraint (14),

2. since λ_3 is assumed to be large and negative (see (26)), the constraint (28) can be satisfied only if $\Omega_\eta/\Omega_T \ll 1$, and

3. to satisfy the XENON100 (1T) constraint we have to impose $|\gamma_2| \lesssim 0.035(0.003)$ for $m_\chi = 135$ GeV.

C. Relic densities of DM

Since our parameter space has been already constrained to a certain amount, we next calculate the relic density of DM, $\Omega_T = \Omega_\chi + \Omega_\eta$. To simplify the situation we have been assuming throughout that η_R^0 and χ are DM particles. In this two-component DM system there are three different thermally averaged cross sections

$$\langle\sigma(\eta_R^0\eta_R^0;\mathrm{SM})v\rangle \ , \ \langle\sigma(\chi\chi;\mathrm{SM})v\rangle \ , \ \langle\sigma(\eta_R^0\eta_R^0;\chi\chi)v\rangle \tag{31}$$

that are relevant for calculating the DM relic density, where SM stands for the SM particles [6]. No semiannihilation $\eta_R^0\chi \to \phi_R(\phi_I)\mathrm{SM}$ is allowed if $m_{\phi_{R(I)}} > m_{\eta_R^0} + m_\chi$. Then the evolution equation for Y, the number density over the entropy density, can be written as [16–19]

$$\begin{aligned}
\frac{dY_{\eta_R^0}}{dx} &= -0.264\ g_*^{1/2}\left[\frac{\mu M_{\rm PL}}{x^2}\right]\Big\{\langle\sigma(\eta_R^0\eta_R^0;\mathrm{SM})v\rangle\left(Y_{\eta_R^0}Y_{\eta_R^0} - \bar{Y}_{\eta_R^0}\bar{Y}_{\eta_R^0}\right) \\
&+\langle\sigma(\eta_R^0\eta_R^0;\chi\chi)v\rangle\left(Y_{\eta_R^0}Y_{\eta_R^0} - \frac{Y_\chi Y_\chi}{\bar{Y}_\chi\bar{Y}_\chi}\bar{Y}_{\eta_R^0}\bar{Y}_{\eta_R^0}\right)\Big\} \ , \qquad (32) \\
\frac{dY_\chi}{dx} &= -0.264\ g_*^{1/2}\left[\frac{\mu M_{\rm PL}}{x^2}\right]\Big\{\langle\sigma(\chi\chi;\mathrm{SM})v\rangle\left(Y_\chi Y_\chi - \bar{Y}_\chi\bar{Y}_\chi\right) \\
&-\langle\sigma(\eta_R^0\eta_R^0;\chi\chi)v\rangle\left(Y_{\eta_R^0}Y_{\eta_R^0} - \frac{Y_\chi Y_\chi}{\bar{Y}_\chi\bar{Y}_\chi}\bar{Y}_{\eta_R^0}\bar{Y}_{\eta_R^0}\right)\Big\} \ , \qquad (33)
\end{aligned}$$

where $\bar{Y}$ is Y in equilibrium, $x = \mu/T$, $1/\mu = 1/m_{\eta_R^0} + 1/m_\chi$, and $T, M_{\rm PL}$ and $g_* = 90$ are the temperature, the Planck mass and the total number of effective degrees of freedom, respectively.

[6] These thermally averaged cross sections are tree-level ones and do not include those into two γ's. Annihilations into two γ's will be separately calculated later on.

Before we solve the evolution equations numerically, we consider what we would expect. As noticed the relic density of η_R^0 will be very small because of large λ_3 and gauge interactions (i.e. large $\langle\sigma(\eta_R^0\eta_R^0;\mathrm{SM})v\rangle$), while the annihilation cross section of χ into the SM particles is suppressed because of (29) (i.e. small $\langle\sigma(\chi\chi;\mathrm{SM})v\rangle$). That is, the DM conversion cross section $\langle\sigma(\eta_R^0\eta_R^0;\chi\chi)v\rangle$ and the mass difference $\Delta m_{\eta\chi} = m_{\eta_R^0} - m_\chi$ will play an important role. Note that the smaller $\Delta m_{\eta\chi}$ is, the larger is the effect of the DM conversion on Ω_χ. To see this more explicitly, we assume that η_R^0 annihilates very fast so that before and at the decoupling of χ the η_R^0 DM is in thermal equilibrium. Then the expression in { } in the rhs of (33) can be written as

$$\left[\langle\sigma(\chi\chi;\mathrm{SM})v\rangle + \langle\sigma(\eta_R^0\eta_R^0;\chi\chi)v\rangle\frac{m_{\eta_R^0}^3}{m_\chi^3}\exp\left(2x\frac{m_\chi^2 - m_{\eta_R^0}^2}{m_\chi m_{\eta_R^0}}\right)\right]\left(Y_\chi Y_\chi - \bar{Y}_\chi\bar{Y}_\chi\right) \ , \qquad (34)$$

which also appears in the co-annihilation of DM with an unstable particle [44] [7]. If $m_\chi^2 - m_{\eta_R^0}^2 < 0$, the effective annihilation cross section of χ is small at low temperature (large x), while it is large at high temperature (small x). Because of the nontrivial interplay between γ_2 and $\Delta m_{\eta\chi}$, it may be possible to obtain a correct relic density $\Omega_T h^2 = 0.1157 \pm 0.0023$ [51]. In Fig. 5 we show the effective annihilation cross section (the expression in [ ] of (34)) as a function of $x = \mu/T$ for $m_{\eta_R^0} = 148$ (dotted), 153 (solid), and 156 (dashed) GeV, where we have fixed the parameters as

$$\lambda_3 \ = \ -1.26 \ , \ \lambda_4 = -0.0205 \ , \ \gamma_3 = 11.3 \ , \qquad (35)$$

$$m_{\eta^\pm} \ = \ m_{\eta_I^0} = m_{\eta_R^0} + 4 \ \mathrm{GeV} \ , \ m_\chi = 135 \ \mathrm{GeV} \ , \ m_h = 125 \ \mathrm{GeV} \ . \qquad (36)$$

As we see from Fig. 5 the effective cross section around the decoupling temperature $x \sim 20$ has a correct size and decreases drastically at low temperature. The effective cross section is normalized to 10^{-26} cm^{3}s^{-1}, because it is the size to obtain the observed relic density of DM. The scalar couplings λ_2, γ_1 and γ_4 do not enter into the cross sections (31), and $\gamma_5, \gamma_6, \gamma_7$ and κ are irrelevant because ϕ is much heavier than η and χ.

In Fig. 6 we show the area in the γ_2–γ_3 plane in which the total relic density $\Omega_T h^2 = 0.1157 \pm 0.0046$ (2σ) with $m_\chi = 135$ GeV can be obtained for $m_{\eta_R^0} = 148$ (black circles), 152 (red diamonds), 153 (red circles), 153.3 (blue circles), 153.5 (green squares), 154 (violet crosses) and 156 (brown triangles) GeV, respectively. The right-handed neutrino masses, M_k, are all 1 TeV, and the Yukawa couplings are chosen to yield $\sum_{ik}|Y_{ik}^\nu|^2 = (10^{-4})^2$. The vertical (black dashed) lines are the upper bounds of γ_2 set by the XENON 100 (right) and 1T (left) experiments (29). From Fig. 6 we can also see that there exits a parameter space with $m_\chi = 135$ GeV, $m_{\eta_R^0} > 153$ GeV, a large $\gamma_3/4\pi$ (between 0.65 and 1.0) and γ_2 satisfying the XENON constraint (29). A large γ_3 is needed to explain the 135 GeV γ-ray line in the Fermi spectrum, as we will see below.

[7] The mechanism has been also used in the model of [40] explaining the monochromatic γ at the Fermi LAT. But the light charged scalar faces a problem in explaining the neutrino mass.

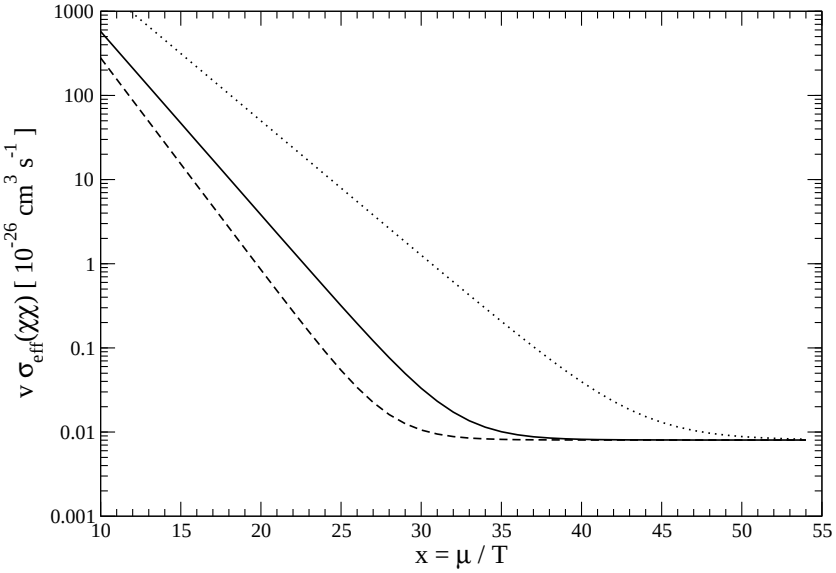

FIG. 5: The effective annihilation cross section (the expression in [ ] of (34)) as a function of $x = \mu/T$ for $m_{\eta_R^0} = 148$ (dotted), 153 (solid), and 156(dashed) GeV with m_χ fixed at 135 GeV.

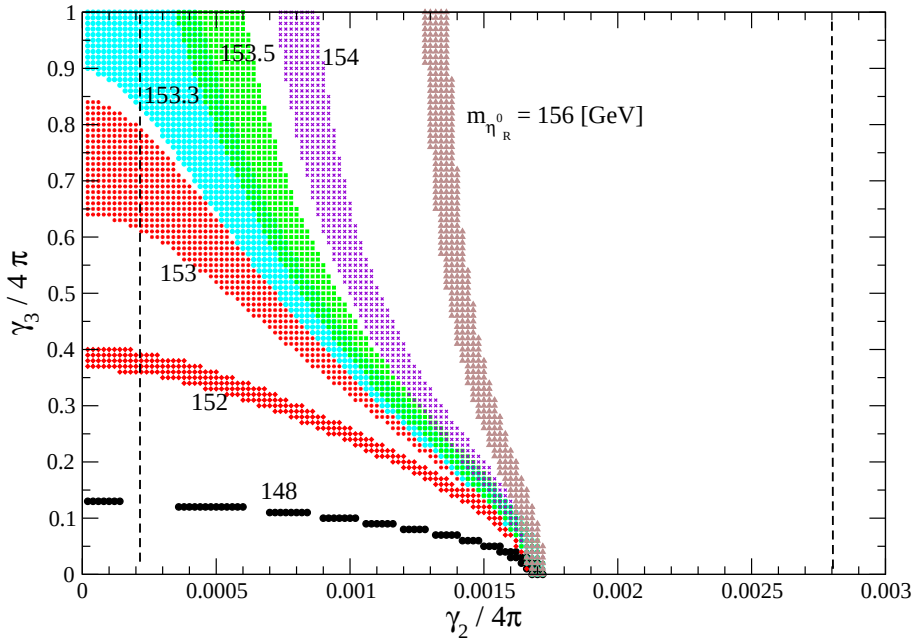

FIG. 6: The area with $\Omega_T h^2 = 0.1157 \pm 0.0046$ (2σ) and $m_\chi = 135$ GeV in the γ_2–γ_3 plane for $m_{\eta_R^0} = 148$ (black circles), 152 (red diamonds), 153 (red circles), 153.3 (blue circles), 153.5 (green squares), 154 (violet crosses) and 156 (brown triangles) GeV, respectively. The vertical (black dashed) lines are the upper bounds of γ_2 set by the XENON 100 (right) and 1T (left) experiments (29).

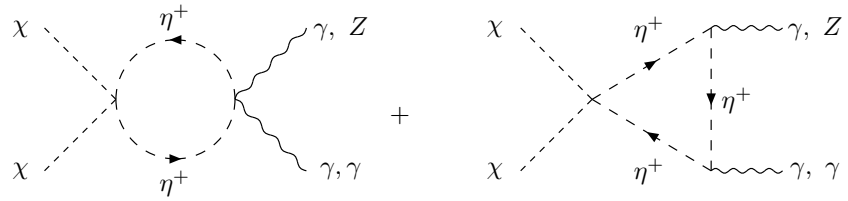

FIG. 7: One-loop diagrams for $\chi\chi \to \gamma\gamma$.

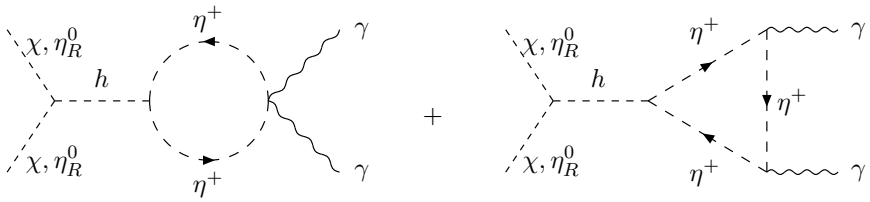

$(2\gamma_2, \lambda_3)v_h \times v_h\lambda_3$

FIG. 8: S-channel diagrams for $h \to \gamma\gamma$.

D. Fermi LAT 135 GeV γ-ray line

Our model contains the coupling between χ and η^+ ($\mathcal{L}_{\eta^\dagger\eta\chi^2} = -\gamma_3\ \eta^\dagger\eta\chi^2$). Because of this coupling there are diagrams in Fig. 7, which produce monochromatic γ lines through the annihilation of χ. We would like to use these diagrams to explain the monochromatic γ-ray line [31, 32, 35, 36] observed at the Fermi LAT [27–30]. There exist also s-channel diagrams with the SM Higgs propagator as shown in Fig. 8. The $h\chi\chi$ coupling is proportional to γ_2, while $h\eta_R^0\eta_R^0$ coupling is proportional to λ_3. The annihilation cross section $\sigma(\eta_R^0\eta_R^0 \to \gamma\gamma)$ is large, because λ_3 is large (see (25) and (26)) [8]. Besides, due to the gauge interactions (see the right diagram of Fig. 4) the relic density of η_R^0 is very small so that the annihilation of the η_R^0 DM can not contribute to the monochromatic γ-ray. Furthermore, because of the same reason, the tree level annihilations of η_R^0 into a pair of W's and Z's, which would contribute to the continuum γ-ray spectrum, are also suppressed. In contrast to this case, the pure gauge interaction (the right diagram of Fig. 4) is absent for the annihilation of χ. The entire annihilations of χ into the SM particles are controlled by the single coupling γ_2, which has to satisfy the constraint (29). Therefore, we may assume that the main contribution to

[8] In [37], $\sigma(\eta_R^0\eta_R^0 \to \gamma\gamma)$ is used to explain the monochromatic γ-ray line, where a fine-tuned cancellation mechanism to suppress the total annihilation cross section of η_R^0 [56] is employed

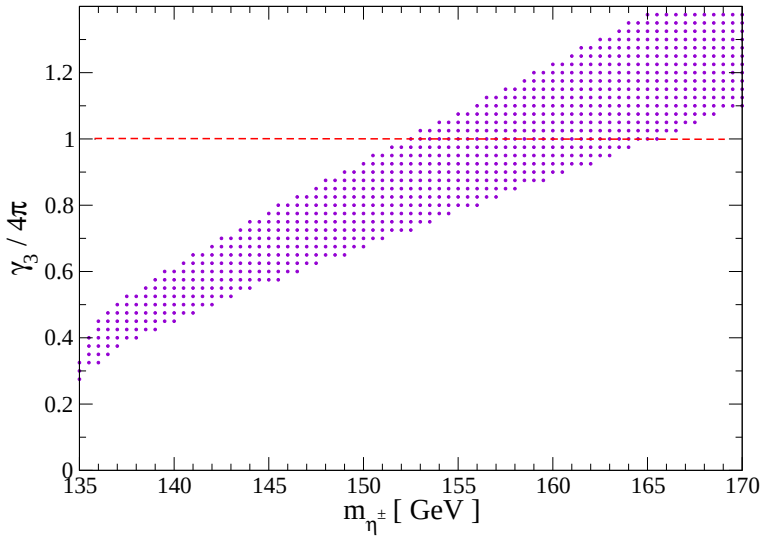

FIG. 9: The area for $\sigma(\chi\chi \to \gamma\gamma)v = (1.27^{+0.37}_{-0.43}) \times 10^{-27}$ cm^{3}s^{-1} in the $m_{\eta^\pm}$–γ_3 plane.

$\sigma(\chi\chi \to \gamma\gamma)$ comes from the one-loop diagrams in Fig. 7 and find

$$\begin{aligned}\sigma(\chi\chi \to \gamma\gamma)v &= \frac{\gamma_3^2\alpha^2 m_\chi^2}{32\pi^3 m_{\eta^\pm}^4}|F_0(m_{\eta^\pm}^2/m_\chi^2)|^2 \\ &\simeq \left[\frac{\gamma_3}{4\pi}\right]^2 \begin{cases} 4.23 \\ 2.66 \\ 1.87 \\ 1.39 \end{cases} \times 10^{-27}\ \text{cm}^3\text{s}^{-1} \text{ for } m_{\eta^\pm} = \begin{cases} 140 \\ 145 \\ 150 \\ 155 \end{cases} \text{ GeV} . \end{aligned} \tag{37}$$

These values should be compared with $(1.27^{+0.37}_{-0.43}) \times 10^{-27}$ cm^{3}s^{-1} [32] for an Einasto DM galactic halo profile, which is the size that could explain the monochromatic γ line observed at the Fermi LAT. So, if $\gamma_3/4\pi$ is large of $O(1)$, the desired value could be obtained. In Fig. 9 we show the area in the $m_{\eta^\pm}$–γ_3 plane in which $\sigma(\chi\chi \to \gamma\gamma)v = (1.27^{+0.37}_{-0.43}) \times 10^{-27}$ cm^{3}s^{-1} can be obtained. If $\eta^\pm$ is lighter than χ, then χ can be annihilated into a pair of $\eta^\pm$. For $m_\chi = 135$ GeV the annihilation cross section becomes $\sigma(\chi\chi \to \eta^+\eta^-)v = (\gamma_3^2/2\pi m_\chi^2)(1 - m_{\eta^\pm}^2/m_\chi^2)^{1/2} \simeq \gamma_3^2(1 - m_{\eta^\pm}^2/m_\chi^2)^{1/2} \times 10^{-22}$ cm^{3}s^{-1}, which is too large to obtain a sufficiently large relic density of χ for a large γ_3 unless $m_\chi \leq m_{\eta^\pm}$. This is why we have to assume that $m_\chi < m_{\eta_R^0}, m_{\eta_I^0}, m_{\eta^\pm}$. Comparing Fig. 9 with Fig. 6, we see that there is an overlapped area, that is, a parameter space in which $\sigma(\chi\chi \to \gamma\gamma)v \simeq 10 \times 10^{-27}$ cm^3 s^{-1} and $\Omega_T h^2 \simeq 0.12$ can be obtained. This is shown in Fig. 10 for $m_{\eta_R^0} = 153.3$ GeV and $m_{\eta^\pm} = m_{\eta_R^0} + 4$ GeV $= 157.3$ GeV.

The same diagrams as in Fig. 7 also produce γZ. The annihilation cross section is given by

$$\sigma(\chi\chi \to \gamma Z)v = \frac{\gamma_3^2\alpha^2 m_\chi^2 \cot^2(2\theta_W)}{16\pi^3 m_{\eta^\pm}^4}|\hat{F}_0(m_{\eta^\pm}^2/m_\chi^2)|^2 , \tag{38}$$

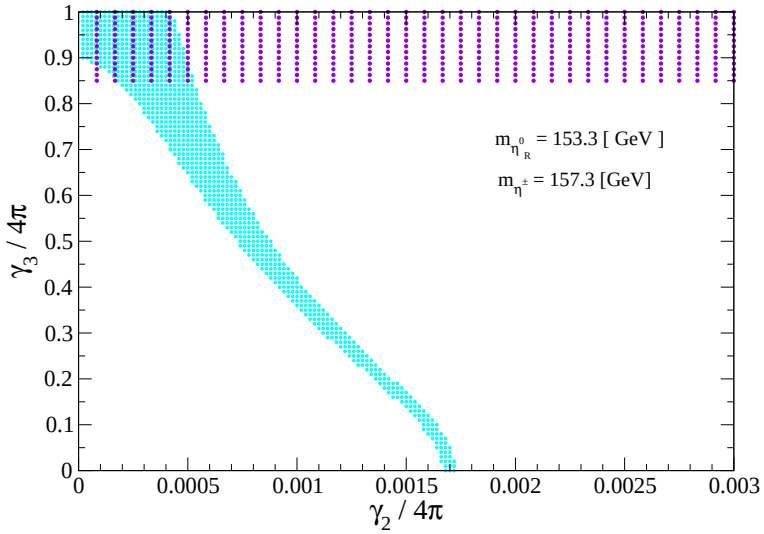

FIG. 10: The parameter space (overlapped area) in which $\sigma(\chi\chi \to \gamma\gamma)v = (1.27^{+0.37}_{-0.43}) \times 10^{-27}$ cm^{3}s^{-1} and $\Omega_T h^2 = 0.1157 \pm 0.0046$ (2σ) can be obtained for $m_{\eta_R^0} = 153.3$ GeV and $m_{\eta^\pm} = m_{\eta_R^0} + 4$ GeV $= 157.3$ GeV.

where

$$\hat{F}_0(\tau_\eta) \;=\; \tau_\eta \left[\frac{1}{2} - \int_0^1 dx \int_0^{1-x} \frac{\tau_\eta - \tau_Z(x^2+y^2) + 4xy(1-\tau_Z/2)}{\tau_\eta + \tau_Z(x^2+y^2) - 4xy(1-\tau_Z/2)} \right] \tag{39}$$

with $\tau_\eta = m^2_{\eta^\pm}/m^2_\chi$ and $\tau_Z = m^2_Z/m^2_\chi$. For $m_{\eta^\pm} = 150$ GeV and $m_\chi = 135$ GeV, for instance, we obtain $\sigma(\chi\chi \to \gamma Z)v = 7.9(\gamma_3/4\pi)^2 \times 10^{-29}$ cm^{3}s^{-1}, which is about 4 % of $\sigma(\chi\chi \to \gamma\gamma)v$. According to [57] this is welcome to explain the Fermi LAT monochromatic γ line.

We also have to satisfy the constraints on the continuum γ and follow the analyses of [57] (see also [58, 59] which give similar constraints). They consider two different constraints, supersaturation constraint and shape constraint, which can be transferred to the upper bound on the ratio of the total annihilation cross section to $\sigma(\chi\chi \to \gamma\gamma)$. Specifically, they consider the constraint on the theoretical ratio

$$R_T^{\rm th} \;=\; \frac{\sigma_T}{2\sigma_{\gamma\gamma} + \sigma_{\gamma Z}} \;, \tag{40}$$

where σ_T is the total annihilation cross section. Since the dominant origins for the continuum γ are $\sigma(\chi\chi \to W^+W^-, ZZ, b\bar{b}, \tau^+\tau^-, \mu^+\mu^-)$, we also consider the individual cross sections and calculate

$$R_\alpha^{\rm th} = \frac{\sigma(\chi\chi \to \alpha)}{2\sigma(\chi\chi \to \gamma\gamma) + \sigma(\chi\chi \to \gamma Z)} \simeq \frac{\sigma(\chi\chi \to \alpha)}{2\sigma(\chi\chi \to \gamma\gamma)} \;, \tag{41}$$

in addition to $R^{\rm th}_{\rm SM} \simeq \sigma(\chi\chi \to {\rm SM})/2\sigma(\chi\chi \to \gamma\gamma)$, where $\alpha = W^+W^-, ZZ, f\bar{f}$. We use the same parameter values given in (36) with $\gamma_2/4\pi = 1.0 \times 10^{-4}$ and $m_{\eta_R^0} = 153.3$ GeV, and we obtain

$$\Omega_\eta h^2 \;=\; 0.981 \times 10^{-5} \;,\; \Omega_\chi h^2 = 0.1197 \;,\; \Omega_T h^2 = 0.1197 \;, \tag{42}$$

and

$$\sigma(\chi\chi \to \gamma\gamma)v \simeq 1.2 \times 10^{-27}\ \mathrm{cm}^3\mathrm{s}^{-1}\ , \tag{43}$$

$$\sigma(\chi\chi \to \mathrm{SM})v \simeq 8.0 \times 10^{-29}\ \mathrm{cm}^3\mathrm{s}^{-1}\ ,\ R^{\mathrm{th}}_{\mathrm{SM}} \simeq 0.06\ , \tag{44}$$

$$\sigma(\chi\chi \to W^+W^-)v \simeq 3.9 \times 10^{-29}\ \mathrm{cm}^3\mathrm{s}^{-1}\ ,\ R^{\mathrm{th}}_{W} \simeq 0.03\ , \tag{45}$$

$$\sigma(\chi\chi \to ZZ)v \simeq 1.7 \times 10^{-29}\ \mathrm{cm}^3\mathrm{s}^{-1}\ ,\ R^{\mathrm{th}}_{Z} \simeq 0.01\ , \tag{46}$$

$$\sigma(\chi\chi \to hh)v \simeq 2.5 \times 10^{-29}\ \mathrm{cm}^3\mathrm{s}^{-1}\ ,\ R^{\mathrm{th}}_{h} \simeq 0.02\ , \tag{47}$$

$$\sigma(\chi\chi \to f\bar{f})v \simeq 1.1 \times 10^{-31}\ \mathrm{cm}^3\mathrm{s}^{-1}\ ,\ R^{\mathrm{th}}_{f} \simeq 10^{-4}\ . \tag{48}$$

These values of R^{th} should satisfy the supersaturation constraint as well as the shape constraint of [57] (see also [58]). There are also constraints coming from the anti-proton-to-proton flux observed by the PAMELA [60]. Anti-protons can be produced by the DM annihilations into the gauge bosons, Higgs bosons and quarks. To explain the PAMELA data, these productions have to be suppressed. The values of R^{th} given in (44)- (48) satisfy all the constraints including the most stringent one $R^{\mathrm{th}} \lesssim 10^{-26}\ \mathrm{cm}^3\mathrm{s}^{-1}$ [57–59, 61–64]. So, the model could explain the monochromatic γ line observed at the Fermi LAT if $m_{\eta^\pm} \simeq 153$ GeV and $\gamma_3/4\pi \sim O(1)$, which is at the border of perturbation theory.

IV. CONCLUSION AND DISCUSSION

In this paper we have proposed a non-supersymmetric model of two-loop radiative seesaw, in which the lepton number is softly broken by a dimension two operator, and the tree-level Dirac mass is forbidden by $Z_2 \times Z_2'$. This discrete symmetry can be used to stabilize two or three dark matter particles. The model contains, in addition to the SM Higgs field, an inert $SU(2)_L$ doublet scalar η and two inert singlet scalars ϕ and χ, and this is a minimal set. We have considered the SM Higgs boson decay into two γ's and found that it is enhanced by η^+ circulating in one-loop diagrams for $h \to \gamma\gamma$. η^+ is also circulating in similar one-loop diagrams contributing to $\chi\chi \to \gamma\gamma$, and we have found that the model has a potential to explain the Fermi LAT 135 GeV γ-ray line.

The mechanism to explain the Fermi LAT 135 GeV γ-ray line in the present model is strongly based the fact that there are at least two particles, particles (which can be DMs, too) and one DM particle of similar masses. Let us briefly outline the mechanism. Annihilation (or decay) of DM into γ's happens always at the loop-level. Those into the SM particles, i.e. W, Z, Higgs boson pairs etc, are usually possible at the tree-level, and they produce continuum γ rays as well as anti-protons. To explain the 135 GeV γ-ray line, we have to suppress these tree-level processes somehow, or enhance the loop process, while keeping the relic abundance of DM at the observed value. In the present model this is realized in the following way. There are two kinds of the tree-level DM annihilations; one into the SM particles and the other into a pair of other DM particles (DM conversion). The slightly

heavier DM (η_R^0 in our model) has large annihilation cross sections both into the SM particles and other DM particles so that its relic density is very small. The 135 GeV γ-ray line comes mainly from the annihilation of the slightly lighter DM (χ in our model). Its annihilation cross section into the SM particles has to be sufficiently small to suppress the continuum γ rays and the production of anti-protons. Although the annihilation of the lighter DM into heavier DM is kinematically forbidden at zero temperature, this process becomes operative at high temperature: The smaller the mass difference of two DM particles is, the more effective is the DM conversion. So, at high temperature the annihilation of the lighter DM is controlled by the mass deference and can be large, but at low temperature, this conversion process practically disappears (see Fig. 5). (For this mechanism to work, the slightly heavier particle does not have to be stable.) It is however important that the lighter one is SM gauge singlet to avoid that the tree-level annihilations are entirely controlled by the SM gauge interactions. (In the present model, the χ DM is not ad hoc introduced.) This is the reason why we can obtain the observed value of the relic density for the lighter DM, although the annihilation cross sections of the lighter DM into the SM particles are very small $\lesssim O(10^{-27})$ cm^{3}s^{-1} in the galaxy.

The annihilation cross sections into the SM particles given in (42), (44)-(48) are obtained without one-loop corrections. Strictly speaking, we should include the one-loop corrections, because the tree-level contributions are so small that the one-loop corrections may be larger than the tree-level corrections. Similarly, the relic densities for Fig. 6 and also (42) have been computed by neglecting the co-annihilation of the DM particles with the charged and CP odd components of η, although we have assumed that their mass differences are not large (i.e. $m_{\eta^\pm} - m_\chi = (17 - 25)$ GeV, $m_{\eta^\pm} - m_{\eta_R^0} = 4$ GeV and $m_{\eta^\pm} = m_{\eta_I^0}$). If the one-loop corrections would change γ_2 effectively by an order of magnitude, then the annihilation cross sections (44)-(48) would change by two orders of magnitude. Even in this case, the supersaturation constraint and shape constraint would be satisfied. The co-annihilations also would effectively increase γ_3. To obtain a realistic relic abundance for the χ DM in that situation, its mass should be slightly increased as one can see from Fig. 6. The one-loop analysis including the co-annihilations is beyond the scope of the present paper, and we will leave it for our future project.

We have assumed throughout that the ϕ is so heavy that it decays into a η_R^0 and a χ. In the case that $m_{\phi_R} < m_\chi + m_{\eta_R^0}$, it becomes the third DM, whose annihilation may be responsible for the second monochromatic γ-ray line in the Fermi data [34]. We leave this question to the future program.

We thank Michael Duerr, Maria Krawczyk and Abdesslam Arhrib for useful discussions. M. A. thanks the Max–Planck–Institut für Kernphysik, Heidelberg for kind hospitality. The work of M. A. is supported in part by the Grant-in-Aid for Scientific Research for Young Scientists (B) (Grant No.22740137), and J. K. is partially supported by the Grant-in-Aid for Scientific Research (C) from the Japan Society for Promotion of Science (Grant

No.22540271).

[1] P. Minkowski, Phys. Lett. B **67** (1977) 421.

[2] M. Gell-Mann, P. Ramond, and R. Slansky, in *Supergravity*, eds. P. van Nieuwenhuizen and D. Z. Freedman (North-Holland, 1979), p. 315; T. Yanagida, in *Proc. of the Workshop on the Unified Theory and the Baryon Number in the Universe*, eds. O. Sawada and A. Sugamoto, KEK Report No. 79-18 (Tsukuba, Japan, 1979), p. 95.

[3] R. N. Mohapatra and G. Senjanovic, Phys. Rev. Lett. **44** (1980) 912.

[4] A. Zee, Phys. Lett. B **93** (1980) 389 [Erratum-ibid. B **95** (1980) 461].

[5] A. Zee, Nucl. Phys. B **264** (1986) 99.

[6] K. S. Babu, Phys. Lett. B **203** (1988) 132.

[7] L. M. Krauss, S. Nasri and M. Trodden, Phys. Rev. D **67** (2003) 085002 [hep-ph/0210389].

[8] E. Ma, Phys. Rev. D **73** (2006) 077301 [hep-ph/0601225].

[9] K. Cheung and O. Seto, Phys. Rev. D **69** (2004) 113009 [hep-ph/0403003].

[10] J. Kubo, E. Ma and D. Suematsu, Phys. Lett. B **642** (2006) 18 [hep-ph/0604114].

[11] M. Aoki, S. Kanemura and O. Seto, Phys. Rev. Lett. **102** (2009) 051805 [arXiv:0807.0361 [hep-ph]]; Phys. Rev. D **80** (2009) 033007 [arXiv:0904.3829 [hep-ph]].

[12] F. Bonnet, M. Hirsch, T. Ota and W. Winter, JHEP **1207** (2012) 153 [arXiv:1204.5862 [hep-ph]].

[13] S. Kanemura and T. Ota, Phys. Lett. B **694** (2010) 233 [arXiv:1009.3845 [hep-ph]].

[14] S. Kanemura, T. Nabeshima and H. Sugiyama, Phys. Lett. B **703** (2011) 66 [arXiv:1106.2480 [hep-ph]].

[15] S. S. C. Law and K. L. McDonald, Phys. Lett. B **713** (2012) 490 [arXiv:1204.2529 [hep-ph]].

[16] F. D'Eramo and J. Thaler, JHEP **1006** (2010) 109 [arXiv:1003.5912 [hep-ph]].

[17] G. Belanger and J.-C. Park, JCAP **1203** (2012) 038 [arXiv:1112.4491 [hep-ph]].

[18] G. Belanger, K. Kannike, A. Pukhov and M. Raidal, JCAP **1204** (2012) 010 [arXiv:1202.2962 [hep-ph]].

[19] M. Aoki, M. Duerr, J. Kubo and H. Takano, Phys. Rev. D **86** (2012) 076015 [arXiv:1207.3318 [hep-ph]].

[20] G. Aad *et al.* [ATLAS Collaboration], Phys. Lett. B **716** (2012) 1 [arXiv:1207.7214 [hep-ex]].

[21] S. Chatrchyan *et al.* [CMS Collaboration], Phys. Lett. B **716** (2012) 30 [arXiv:1207.7235 [hep-ex]].

[22] ATLAS Collaboration, ATLAS-CONF-2012-091.

[23] J. F. Gunion, H. E. Haber, G. L. Kane and S. Dawson, Front. Phys. **80** (2000) 1.

[24] A. G. Akeroyd, M. A. Diaz and M. A. Rivera, Phys. Rev. D **76** (2007) 115012 [arXiv:0708.1939 [hep-ph]].

[25] A. Arhrib, R. Benbrik and N. Gaur, Phys. Rev. D **85** (2012) 095021 [arXiv:1201.2644 [hep-ph]].

[26] B. Swiezewska and M. Krawczyk, arXiv:1212.4100 [hep-ph].

[27] W. B. Atwood *et al.* [LAT Collaboration], Astrophys. J. **697** (2009) 1071 [arXiv:0902.1089 [astro-ph.IM]].

[28] A. A. Abdo, M. Ackermann, M. Ajello, W. B. Atwood, L. Baldini, J. Ballet, G. Barbiellini and D. Bastieri *et al.*, Phys. Rev. Lett. **104** (2010) 091302 [arXiv:1001.4836 [astro-ph.HE]].

[29] M. Ackermann *et al.* [LAT Collaboration], Phys. Rev. D **86** (2012) 022002 [arXiv:1205.2739 [astro-ph.HE]].

[30] Fermi-LAT Collaboration, http://fermi.gsfc.nasa.gov/science/mtgs/symposia/2012/program/fri/AAlbert.

[31] T. Bringmann, X. Huang, A. Ibarra, S. Vogl and C. Weniger, JCAP **1207** (2012) 054 [arXiv:1203.1312 [hep-ph]].

[32] C. Weniger, JCAP **1208** (2012) 007 [arXiv:1204.2797 [hep-ph]].

[33] E. Tempel, A. Hektor and M. Raidal, JCAP **1209**, 032 (2012) [Addendum-ibid. **1211**, A01 (2012)] [arXiv:1205.1045 [hep-ph]].

[34] A. Rajaraman, T. M. P. Tait and D. Whiteson, JCAP **1209** (2012) 003 [arXiv:1205.4723 [hep-ph]].

[35] M. Su and D. P. Finkbeiner, arXiv:1206.1616 [astro-ph.HE].

[36] M. Su and D. P. Finkbeiner, arXiv:1207.7060 [astro-ph.HE].

[37] A. Biswas, D. Majumdar, A. Sil and P. Bhattacharjee, arXiv:1301.3668 [hep-ph].

[38] F. D'Eramo, M. McCullough and J. Thaler, arXiv:1210.7817 [hep-ph].

[39] P. -H. Gu, arXiv:1301.4368 [hep-ph].

[40] S. Baek, P. Ko and E. Senaha, arXiv:1209.1685 [hep-ph].

[41] Y. Bai, V. Barger, L. L. Everett and G. Shaughnessy, arXiv:1212.5604 [hep-ph].

[42] J. M. Cline, Phys. Rev. D **86** (2012) 015016 [arXiv:1205.2688 [hep-ph]].

[43] L. Wang and X. -F. Han, Phys. Rev. D **87** (2013) 015015 [arXiv:1209.0376 [hep-ph]].

[44] K. Griest, D. Seckel, Phys. Rev. **D43** (1991) 3191-3203.

[45] G. Passarino and M. J. G. Veltman, Nucl. Phys. B **160**, 151 (1979).

[46] E. Ma and M. Raidal, Phys. Rev. Lett. **87** (2001) 011802 [Erratum-ibid. **87** (2001) 159901] [arXiv:hep-ph/0102255].

[47] K. Hayasaka, arXiv:1010.3746 [hep-ex].

[48] J. Beringer *et al.* [Particle Data Group Collaboration], Phys. Rev. D **86** (2012) 010001.

[49] R. Barbieri, L. J. Hall and V. S. Rychkov, Phys. Rev. D **74** (2006) 015007 [arXiv:hep-ph/0603188].

[50] J. R. Ellis, A. Ferstl and K. A. Olive, Phys. Lett. B **481** (2000) 304 [arXiv:hep-ph/0001005].

[51] G. Hinshaw, D. Larson, E. Komatsu, D. N. Spergel, C. L. Bennett, J. Dunkley, M. R. Nolta and M. Halpern *et al.*, arXiv:1212.5226 [astro-ph.CO].

[52] E. Aprile *et al.* [XENON100 Collaboration], Phys. Rev. Lett. **109** (2012) 181301 [arXiv:1207.5988 [astro-ph.CO]].

[53] E. Aprile [XENON1T Collaboration], arXiv:1206.6288 [astro-ph.IM].

[54] L. Lopez Honorez, E. Nezri, J. F. Oliver and M. H. G. Tytgat, JCAP **0702** (2007) 028 [arXiv:hep-ph/0612275].

[55] E. M. Dolle and S. Su, Phys. Rev. D **80** (2009) 055012 [arXiv:0906.1609 [hep-ph]].

[56] L. Lopez Honorez and C. E. Yaguna, JCAP **1101** (2011) 002 [arXiv:1011.1411 [hep-ph]].

[57] T. Cohen, M. Lisanti, T. R. Slatyer and J. G. Wacker, JHEP **1210** (2012) 134 [arXiv:1207.0800 [hep-ph]].

[58] W. Buchmuller and M. Garny, JCAP **1208** (2012) 035 [arXiv:1206.7056 [hep-ph]].

[59] G. Belanger, C. Boehm, M. Cirelli, J. Da Silva and A. Pukhov, JCAP **1211**, 028 (2012) [arXiv:1208.5009 [hep-ph]].

[60] O. Adriani *et al.* [PAMELA Collaboration], Phys. Rev. Lett. **105** (2010) 121101 [arXiv:1007.0821 [astro-ph.HE]].

[61] A. Ibarra and D. Tran, JCAP **0807** (2008) 002 [arXiv:0804.4596 [astro-ph]].

[62] F. Donato, D. Maurin, P. Brun, T. Delahaye and P. Salati, Phys. Rev. Lett. **102** (2009) 071301 [arXiv:0810.5292 [astro-ph]].

[63] W. Buchmuller, A. Ibarra, T. Shindou, F. Takayama and D. Tran, JCAP **0909** (2009) 021 [arXiv:0906.1187 [hep-ph]].

[64] M. Asano, T. Bringmann, G. Sigl and M. Vollmann, arXiv:1211.6739 [hep-ph].